Applied Artificial Intelligence
An International Journal

ISSN: 0883-9514 (Print) 1087-6545 (Online) Journal homepage: https://www.tandfonline.com/loi/uaai20

On Composite Leader–follower Formation Control for Wheeled Mobile Robots with Adaptive Disturbance Rejection

Sida Lin, Ruiming Jia, Ming Yue & Yuan Xu

To cite this article: Sida Lin, Ruiming Jia, Ming Yue & Yuan Xu (2019) On Composite Leader–follower Formation Control for Wheeled Mobile Robots with Adaptive Disturbance Rejection, Applied Artificial Intelligence, 33:14, 1306-1326, DOI: 10.1080/08839514.2019.1685182

To link to this article: https://doi.org/10.1080/08839514.2019.1685182

APPLIED ARTIFICIAL INTELLIGENCE
2019, VOL. 33, NO. 14, 1306–1326
https://doi.org/10.1080/08839514.2019.1685182

Taylor & Francis
Taylor & Francis Group

On Composite Leader–follower Formation Control for Wheeled Mobile Robots with Adaptive Disturbance Rejection

Sida Lin[a], Ruiming Jia[b], Ming Yue[b,c], and Yuan Xu[b]

[a]School of Control Science and Engineering, Dalian University of Technology, Dalian, China; [b]School of Automotive Engineering, Dalian University of Technology, Dalian, China; [c]State Key Laboratory of Robotics and System, Harbin Institute of Technology, Harbin, China

ABSTRACT

This paper proposes a composite control strategy for the formation control of a group of wheeled mobile robots (WMRs) by taking full advantages of model predictive control (MPC) and adaptive terminal sliding mode control (ATSMC) techniques. To begin with, in order to confirm the formulation stability of leader-follow system, a formation controller based on MPC scheme is proposed to assure the desired formation and the position consistency of followers. Afterward, a dynamic controller based on ATSMC scheme is developed for the leader to observe and then compensate the external disturbance as soon as possible. With the presented composite control strategy, not only the desired formation but also trajectory tracking can be simultaneously achieved, in addition to offering the leader to be robust and adaptive to overcome the uncertain disturbances. At last, the simulation results illustrate the feasibility and effectiveness of the proposed control strategy.

Introduction

Recently, the multi-robot formation control attracts much attentions due to its excellent performance in many areas, such as resource detection, rescue, and cooperative transportation, see e.g. Cui et al. (2010), Xiao et al. (2016), Wang, Li, and Shi (2014), Wang, Wang, and Peng (2017), Yu, Chen, and Cao (2010), Qin, Gao, and Zheng (2012), Ren and Sorensen (2008), Yoo (2017), and reference therein. Among existing formation control modes, the leader-follower approach is a significant control method since its simple design pattern, where one robot is chosen as a leader which leads the formation to move along a desired trajectory, and the others are chosen as followers to track the leader with desired formation. As for a leader-follower formation system, the basic requirements yield twofold: (1) the followers can track leader and maintain the desired formation; (2) the leader is able to track the desired trajectory rapidly, even if there exists uncertain

CONTACT Ming Yue yueming@dlut.edu.cn School of Automotive Engineering, Dalian University of Technology, Dalian, China

Color versions of one or more of the figures in the article can be found online at www.tandfonline.com/uaai.

disturbance, thereby guaranteeing the followers' tracking maneuvres as accurately as possible.

At first, an effective and efficient formation controller needs to be found based on an appropriate formation model to achieve not only followers' posture tracking but also entire formation configuration stability. For these purposes, the control-oriented formation model should be concerned with proper state variables including followers' posture and formation configuration messages; based on such an appropriate model, it is possible to present a feasible control strategy to assure the multi-objective coordinated effects. In the existing references, many literatures have studied on the formation controllers based on their reasonable system models/formulations. For example, Peng et al. established a formation model with the relative distance and the relative angle between leader and followers as state variables, clearly revealing the position relationship between leader and followers in the formation Peng et al. (2013). After that, in Xiao et al. (2016) a formation model that considers the orientation of followers was proposed, and simultaneously the consistency of followers was taken into consideration on the basis of the desired formation as well. By synthetically analyzing the existing state variable selecting methods, this paper intends to adopt three variables to describe the full information of follower, that is, the heading angle, the distance and orientation angle, all of which are relative to the leader. Once the three variables are confirmed, the posture of the follower and formation configuration is determined afterward. Besides, as for the design of the formation controller, there exists considerable control methods such as graph theory Qin and Yu (2013), Hong, Hu, and Gao (2006), Sun and Wang (2012), feedback linearization method Wang et al. (2016, 2017), Zhao, Yang, and Zong (2016) and backstepping scheme Peng et al. (2016), Yang et al. (2019) and Sun et al. (2019). Compared with above control methods, the model predictive control (MPC) can avoid the selection of a complex Lyapunov candidate functions, with great advantages at dealing the multiple constraints problem Ke et al. (2017), Zhang, Zhuang, and Braatz (2016), Li et al. (2016). Based on the aforementioned advantages, a MPC-based formation controller is used here to achieve the formation control. Apart from realizing the previously multi-objective coordinated control effects, the distance and speed constraints for both formation and mobile robots can be guaranteed readily by the proposed MPC-based controller.

Next, considering the mobile robot formation often runs in unstructured environments such as rough roads and slippery outdoor, the leader will inevitably be affected by external disturbance, and frequently results in deviating from the desired trajectory. Therefore, it makes most sense to enhance the stability and anti-disturbance ability, especially for the leader which will provide explicit reference trajectory for the following agents. Meanwhile, due to the usually force form of the external disturbance,

a double closed-loop control strategy that contains an outer loop and an inner loop for the leader is proposed to enhance the multilevel movement robustness of the leader. In this regard, the outer loop contains a kinematic model of the leader and a MPC-based motion controller for the leader to realize the tracking to the desired trajectory; the inner loop consists of a dynamic model and a dynamic controller which considers the effect of the external disturbance. Moreover, in the chosen of the dynamic controller, the terminal sliding mode control (TSMC) is employed since its the characteristics of quickly responding and being converging to error within a finite time, see e.g., Hu et al. (2019), Xiao et al. (2016), Pan et al. (2015), Li, Shi, and Yao (2017), Xu, Hu, and Zhang (2017), Hu et al. (2018), thus this paper proposes a TSMC technique to construct the dynamic controller. In addition, because the real external disturbance cannot be obtained in practice, an adaptive law for the external disturbance is established by combining the TSMC-based controller, such that the ATSMC-based dynamic controller can achieve the observation and compensation capabilities to the disturbance, and then to enhance the stability and anti-disturbance ability of the leader.

To sum up, this paper devotes to propose a composite control strategy to realize multi-objective coordinate control purposes. Specifically, a formation model that considers the specific posture of followers, and a MPC-based formation controller that achieves the desired formation as well as tracking the leader with a satisfactory control performance. Particularly, an ATSMC-based dynamic controller is presented for the leader to enhance its stability and anti-disturbance ability, by which the tracking errors can be converged in a finite time with robust capability.

The paper is organized as follows. In Section 2, the kinematic and dynamic models of the wheeled mobile robot (WMR) formation are established, respectively. In Section 3, the control structure, control objective and controller design are presented. In Section 4, the simulation results are discussed to validate the effectiveness and feasibility of the proposed control strategy. Conclusion is summarized in Section 5.

Problem Description

WMR Kinematic and Dynamic Formulations

Consider a group of z nonholonomic WMRs. The posture of i-th ($1 \leq i \leq z$) WMR (named as $\mathcal{R}_i$) in Cartesian coordinate system XOY is described by $q_i = [x_i, y_i, \theta_i]^T$, where (x_i, y_i) denotes the centroid of the robot $\mathcal{R}_i$, and θ_i is the heading angle with the positive direction of anti-clockwise. With the assumptions of pure rolling toward forward and no slipping along the lateral directions, respectively, the nonholonomic constraint of the robot $\mathcal{R}_i$ can be express as

$$-\dot{x}_i \sin\theta_i + \dot{y}_i \cos\theta_i - d\dot{\theta}_i = 0 \tag{1}$$

where d is the distance from center of rear axle to the centroid of the robot $\mathcal{R}_i$. From the nonholonomic constraint (1), the kinematic model of the robot $\mathcal{R}_i$ is given by

$$\dot{q}_i \quad = S(q_i)v_i = \begin{bmatrix} \cos\theta_i & -d\sin\theta_i \\ \sin\theta_i & d\cos\theta_i \\ 0 & 1 \end{bmatrix} \begin{bmatrix} v_i \\ \omega_i \end{bmatrix} \tag{2}$$

where v_i and ω_i are the liner and angular velocities of the robot $\mathcal{R}_i$, respectively. The dynamic model of a nonholonomic WMR system at the present of uncertain disturbance can be described by

$$M(q_i)\ddot{q}_i + C(q_i, \dot{q}_i)\dot{q}_i + F_d = B(q_i)\tau_i + A^T(q_i)\lambda \tag{3}$$

where $M(q_i)$ is the inertia matrix of the robot $\mathcal{R}_i$, $C(q_i, \dot{q}_i)$ is the Coriolis matrix, F_d is the disturbance matrix, $B(q_i)$ is the control input transformation matrix, τ_i is the control input vector, $A(q_i)$ is the nonholonomic constraint matrix and λ is the lagrange multiplier. After eliminating nonholonomic constraint of (3) with $S(q_i)$, one can get a reduced-order dynamic model of WMR as

$$\bar{M}(q_i)\dot{v}_i = \bar{B}(q_i)\tau_i - F \tag{4}$$

where

$$\bar{M}(q_i) = \begin{bmatrix} m & 0 \\ 0 & J - md^2 \end{bmatrix}, \bar{B}(q_i) = \frac{1}{r}\begin{bmatrix} 1 & 0 \\ 0 & R \end{bmatrix}, F = \begin{bmatrix} f_v \\ f_\omega \end{bmatrix}, \tau_i = \begin{bmatrix} \tau_v \\ \tau_\omega \end{bmatrix} = \begin{bmatrix} \tau_l + \tau_r \\ \tau_l - \tau_r \end{bmatrix}$$

where m and J are the mass and the rotational inertia of robot, r and R are wheel radius and half distance of the axle, τ_l and τ_r are the torque of left and right wheel, f_v and f_ω mean equivalent disturbance for the robot longitudinal and steering subsystems, respectively. More details about these formulation can be referred to Refs. Yue et al. (2014, 2015).

Leader-Follower Formation Model

A leader-follower formation is shown in Figure 1. Defining generalized coordinate vector $P_f = [x_f, y_f, \theta_f]^T$ as the position of follower robot $\mathcal{R}_f$, where (x_f, y_f) and θ_f are the centroid coordinate and heading angle of $\mathcal{R}_f$, respectively. Based on the geometric position relationship, one can obtain that

$$P_f = \begin{bmatrix} x_f \\ y_f \\ \theta_f \end{bmatrix} = \begin{bmatrix} x_l - d\cos\theta_l + \rho_{lf}\cos(\psi_{lf} + \theta_l) \\ y_l - d\sin\theta_l + \rho_{lf}\sin(\psi_{lf} + \theta_l) \\ \theta_f \end{bmatrix} \tag{5}$$

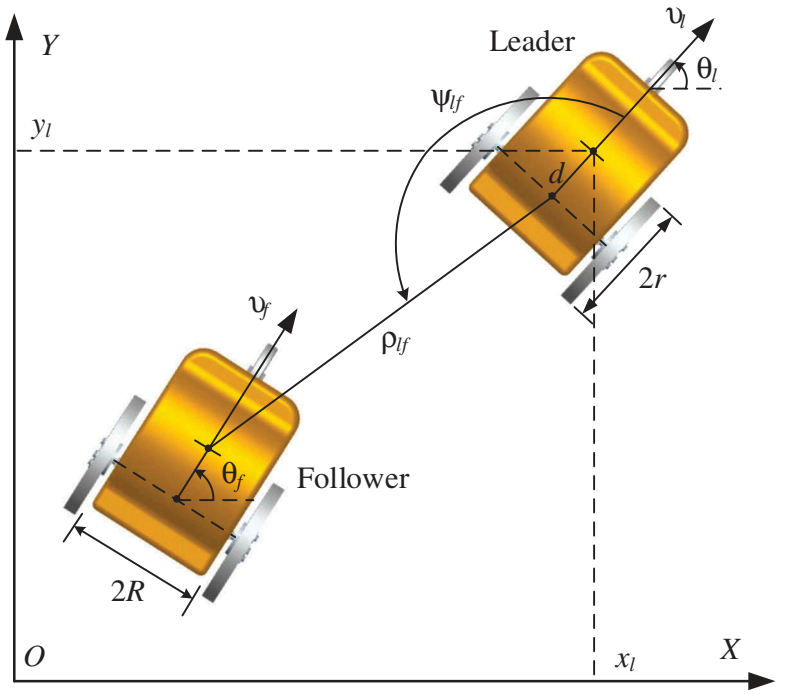

Figure 1. Leader–Follower formation model.

where (x_l, y_l) and θ_l are the centroid coordinate and heading angle of the leader robot $\mathcal{R}_l$, ρ_{lf} and ψ_{lf} are the separation and the bearing angle between $\mathcal{R}_f$ and $\mathcal{R}_l$, respectively. From (5), it follows that

$$\begin{cases} \rho_{lfx} = x_l - d\cos\theta_l - x_f = -\rho_{lf}\cos(\psi_{lf} + \theta_l) \\ \rho_{lfy} = y_l - d\sin\theta_l - y_f = -\rho_{lf}\sin(\psi_{lf} + \theta_l) \end{cases} \tag{6}$$

The fact that (6) should satisfy the Pythagorean theorem, that is

$$\rho_{lf} = \sqrt{\rho_{lfx}^2 + \rho_{lfy}^2} \tag{7}$$

Differentiating (6) with respect to time along (2) trajectory yields

$$\begin{cases} \dot{\rho}_{lfx} = v_l\cos\theta_l - v_f\cos\theta_f + d\omega_f\sin\theta_f \\ \dot{\rho}_{lfy} = v_l\sin\theta_l - v_f\sin\theta_f - d\omega_f\cos\theta_f \end{cases} \tag{8}$$

Also, taking derivatives of (7) along (8) results in

$$\dot{\rho}_{lf} = v_f\cos(\psi_{lf} + \beta_{lf}) - v_l\cos\psi_{lf} + d\omega_f\sin(\psi_{lf} + \beta_{lf}) \tag{9}$$

where $\beta_{lf} = \theta_l - \theta_f$. From geometric relationship of the bearing angle ψ_{lf} between $\mathcal{R}_f$ and $\mathcal{R}_l$, it holds that

$$\psi_{lf} = \arctan\left(\frac{\rho_{lfy}}{\rho_{lfx}}\right) - \theta_l + \pi \tag{10}$$

Furthermore, by taking derivatives of (10) along the trajectory (8), it results in

$$\dot{\psi}_{lf} = \frac{1}{\rho_{lf}}(v_l \sin\psi_{lf} - v_f \sin(\psi_{lf} + \beta_{lf}) + d\omega_f \cos(\psi_{lf} + \beta_{lf})) - \omega_l \tag{11}$$

Defined leader-follower formation control state vector as $\mathcal{X} = [\rho_{lf}, \psi_{lf}, \beta_{lf}]^T$, and the control input as $u = [v_f, \omega_f]^T$, a leader-follower formation model (referred to Xiao et al. (2016)) can be express as

$$\dot{\mathcal{X}} = f(x,u) = \left[\dot{\rho}_{lf}, \dot{\psi}_{lf}, \dot{\beta}_{lf}\right]^T = \begin{bmatrix} v_f \cos(\psi_{lf} + \beta_{lf}) - v_l \cos\psi_{lf} + d\omega_f \sin(\psi_{lf} + \beta_{lf}) \\ \frac{1}{\rho_{lf}}(v_l \sin\psi_{lf} - v_f \sin(\psi_{lf} + \beta_{lf}) + d\omega_f \cos(\psi_{lf} + \beta_{lf})) - \omega_l \\ \omega_l - \omega_f \end{bmatrix} \tag{12}$$

Control System Synthesis

Control Structure and Objectives

The presented composite control structure, as shown in Figure 2, is in essence a layered structure, by which a comprehensive coordinated multi-objectives including both vehicle kinematics and dynamics performance can be achieved correspondingly. Here, as for the leader, a composite control strategy comprised with a MPC-based motion controller and an ATSMC-

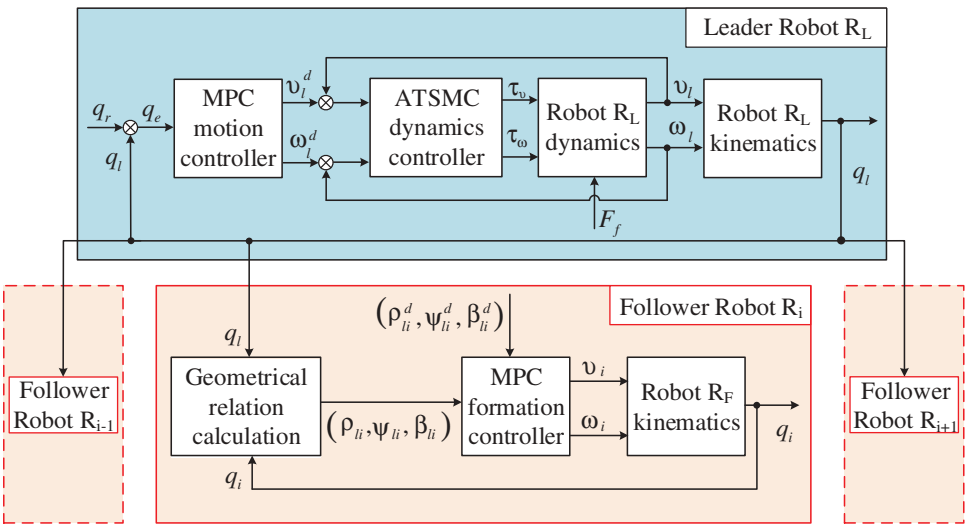

Figure 2. Control structure of the presented system.

based dynamics controller is put forward. As for the followers, a state constrained MPC formation controller is designed to track the leader, maintaining the desired formation between the leader and the followers.

Notice that the leader, which offers reference trajectory for the followers, must be paid more attention since once unfavorable effects take place in leader agent, a series of follower ones will all undergo drastic adjustments. Therefore, a composite control with much more controlling consumption is provided for the leader to obtain better movement performance. For comparison, as for the follower robot, one is mainly concerned with its configuration constraint, such that a constrained MPC algorithm is determined to be utilized to control the follower agents. To sum up, the control objectives of the presented controllers can be summarized as follows

- For motion controller, find a control law $v_l^d = [v_l^d, \omega_l^d]^T$, such that $q_l = [x_l, y_l, \theta_l]^T \rightarrow q_r = [x_r, y_r, \theta_r]^T$;
- For dynamic controller, find a control law $\tau = [\tau_v, \tau_\omega]^T$, such that $v_l^d = [v_l^d, \omega_l^d]^T \rightarrow v_l^r = [v_l^r, \omega_l^r]^T$;
- For formation controller, find a control law $v_i = [v_i, \omega_i]^T$, such that $\mathcal{X} = [\rho_{li}, \psi_{li}, \beta_{li}]^T \rightarrow \mathcal{X}^d = [\rho_{li}^d, \psi_{li}^d, \beta_{li}^d]^T$.

Remark 3.1 The symbol mentioned above q_l and q_r are leader's actual trajectory and the reference ones, respectively. The symbol v_l^r and v_l^d represent the leader's reference velocity and desired velocity, where the reference one v_l^r is decided by the differential of the reference trajectory, and the desired velocity v_l^d obtained by the MPC motion controller and is also the desired value for the ATSMC dynamics controller to tracking. The symbol $\mathcal{X}$ and $\mathcal{X}^d$ are the formation state and their desired values, in which the desired formation state $\mathcal{X}^d = [\rho_{li}^d, \psi_{li}^d, \beta_{li}^d]^T$ will given in advance.

MPC-based motion/formation controller

The leader can be considered as a mass point when designing the motion controller. Besides, due to the simple calculation procedures and good real-time characteristics of linear MPC possesses, this technique is adopted here to design motion controller. By linearization, discretization and state amplification, the motion predictive model and the formation predictive model, respectively, can be obtained as follows

$$\begin{cases} \bar{x}_l(k+1) = \bar{A}_{lT}\bar{x}_l(k) + \bar{B}_{lT}\Delta u_l(k) \\ \bar{y}_l(k) = \bar{C}_{lT}\bar{x}_l(k) \end{cases} \tag{13}$$

$$\begin{cases} \bar{x}_i(k+1) = \bar{\mathcal{A}}_{iT}\bar{x}_i(k) + \bar{\mathcal{B}}_{iT}\Delta u_i(k) \\ \bar{y}_i(k) = \bar{\mathcal{C}}_{iT}\bar{x}_i(k) \end{cases} \tag{14}$$

where subscript l and i denote the leader and formation control for the i-th follower, respectively, thus the other matrices can be achieved as follows

$$\bar{\mathcal{A}}_{lT} = \begin{bmatrix} \mathcal{A}_{lT} & \mathcal{B}_{lT} \\ 0_{2\times 3} & I_2 \end{bmatrix} \in \mathbb{R}^{5\times 5}, \bar{\mathcal{B}}_{lT} = \begin{bmatrix} \mathcal{B}_{lT} \\ I_2 \end{bmatrix} \in \mathbb{R}^{5\times 2}, \bar{\mathcal{C}}_{lT} = [\, I_3, 0\,] \in \mathbb{R}^{3\times 5},$$

$$\mathcal{A}_{lT} = \begin{bmatrix} 0 & 0 & -v_l^d \sin\theta_l^d \\ 0 & 0 & v_l^d \cos\theta_l^d \\ 0 & 0 & 0 \end{bmatrix}, \mathcal{B}_{lT} = \begin{bmatrix} \cos\theta_l^d & 0 \\ \sin\theta_l^d & 0 \\ 0 & 1 \end{bmatrix};$$

$$\bar{\mathcal{A}}_{iT} = \begin{bmatrix} \mathcal{A}_{iT} & \mathcal{B}_{iT} \\ 0_{2\times 3} & I_2 \end{bmatrix} \in \mathbb{R}^{5\times 5}, \bar{\mathcal{B}}_{iT} = \begin{bmatrix} \mathcal{B}_{iT} \\ I_2 \end{bmatrix} \in \mathbb{R}^{5\times 2}, \bar{\mathcal{C}}_{iT} = [\, I_3, 0\,] \in \mathbb{R}^{3\times 5},$$

$$\mathcal{A}_{iT} = \begin{bmatrix} 0 & a_{i12} & a_{i13} \\ a_{i21} & a_{i22} & a_{i23} \\ 0 & 0 & 0 \end{bmatrix}, \mathcal{B}_{iT} = \begin{bmatrix} b_{i11} & b_{i12} \\ b_{i21} & b_{i22} \\ 0 & -1 \end{bmatrix}.$$

where T denotes sampling time, and the specific parameters are given by

$$a_{i12} = -v_i^d \sin(\psi_{li}^d + \beta_{li}^d) + v_l \sin\psi_{li}^d + d\omega_i^d \cos(\psi_{li}^d + \beta_{li}^d),$$

$$a_{i13} = -v_i^d \sin(\psi_{li}^d + \beta_{li}^d) + d\omega_i^d \cos(\psi_{li}^d + \beta_{li}^d),$$

$$a_{i21} = -\frac{1}{(\rho_{li}^d)^2}(v_l \sin\psi_{li}^d - v_i^d \sin(\psi_{li}^d + \beta_{li}^d) + d\omega_i^d \cos(\psi_{li}^d + \beta_{li}^d)),$$

$$a_{i22} = \frac{1}{\rho_{li}^d}(v_l \cos\psi_{li}^d - v_i^d \cos(\psi_{li}^d + \beta_{li}^d) - d\omega_i^d \sin(\psi_{li}^d + \beta_{li}^d)),$$

$$a_{i23} = \frac{1}{\rho_{li}^d}(-v_i^d \cos(\psi_{li}^d + \beta_{li}^d) - d\omega_i^d \sin(\psi_{li}^d + \beta_{li}^d)),$$

$$b_{i11} = \cos(\psi_{li}^d + \beta_{li}^d), b_{i12} = d\sin(\psi_{li}^d + \beta_{li}^d),$$

$$b_{i21} = -\frac{1}{\rho_{li}^d}\sin(\psi_{li}^d + \beta_{li}^d), b_{i22} = \frac{1}{\rho_{li}^d} d\cos(\psi_{li}^d + \beta_{li}^d).$$

Here, to prevent the control output torque mutation caused by the torque mutation of driving motor, it is essential to constraint the speed and speed increment during the control process. The considered constraints can be introduced as the following forms

$$\begin{aligned} v_{\min} \le v(k) \le v_{\max}, \quad & k = 0, 1, \cdots, N_c - 1 \\ \Delta v_{\min} \le \Delta v(k) \le \Delta v_{\max}, \quad & k = 0, 1, \cdots, N_c - 1 \end{aligned} \tag{15}$$

where $v_{\min}$ and $v_{\max}$ are lower and upper bounds of the control input; $\Delta v_{\min}$ and $\Delta v_{\max}$ are lower and upper bounds of the control input increment, respectively.

Moreover, the objective of the motion and formation control requires the system outputs follow the reference values as closely as possible, in addition to costing the minimum control efforts. Considering the prediction model, using the velocity increment as the control input, thus at some transient sampling time k, the cost function can be expressed as

$$\mathcal{J}(\bar{x}(k), \Delta v(k), v(k-1)) = \left\|\mathcal{Y}^d(k) - \mathcal{Y}^d(k)\right\|_Q^2 - \|\Delta v(k)\|_R^2 + \xi\varepsilon^2 \tag{16}$$

where $\mathcal{Y}^d(k)$ represents the reference trajectory given by earth-fixed frame; $\mathcal{Y}(k)$ is predictive output; $Q \in \mathbb{R}^{3\times3}$ and $R \in \mathbb{R}^{2\times2}$ are introduced symmetric positive definite matrices, presenting the weight factors of the control target and control input, respectively; ε and ξ presenting the relaxation factor and its weight factor, respectively.

For motion control system (13), the original optimization problem (16) can be rewritten as a quadratic programming (QP) problem as follows

$$\begin{array}{ll} \min & \mathcal{J}_l(\bar{x}_l(k), \Delta v_l(k), v_l(k-1)) = \frac{1}{2}\Delta v_l(k)^T \mathcal{H}_l \Delta v_l(k) + \Theta_l^T \Delta v_l(k) \\ s.t. & \Delta v_{\min} \le \Delta v_l(k) \le \Delta v_{\max} \\ & v_{\min} \le \bar{I}\Delta v_{lk}(k) + 1_{N_c} \otimes v_l(k-1) \le v_{\max} \end{array} \tag{17}$$

where

$$\mathcal{H}_l = 2\left(\Psi_l^T Q_l \Psi_l + R_l\right) \in \mathbb{R}^{2N_c\times2N_c}$$

$$\Theta_l = 2\Psi Q_{ll}\left(\mathcal{Y}_l^d(k) - \mathcal{Y}_l(k)\right) \in \mathbb{R}^{2N_c}$$

For formation control system (14), not only the velocity and its increment should be constrained, but also the state output need to be restricted to enhance the stability of the formation, simultaneously. The state output constraint of formation system can be expressed as

$$\mathcal{Y}_{\min} \le \mathcal{Y} \le \mathcal{Y}_{\max} \tag{18}$$

where $\mathcal{Y}_{\min} = [\rho_{\min}, \psi_{\min}, \beta_{\min}]^T$ and $\mathcal{Y}_{\max} = [\rho_{\max}, \psi_{\max}, \beta_{\max}]^T$. Combining objective function (16) with constraints (15) and (18), constraint optimization problem can be transformed to QP problem as follows

$$\begin{array}{ll} \min & \mathcal{J}_i(\bar{x}_i(k), \Delta v_i(k), v_i(k-1)) = \frac{1}{2}\Delta v_i(k)^T \mathcal{H}_i \Delta v_i(k) + \Theta_i^T \Delta v_i(k) \\ s.t. & \Delta v_{\min} \le \Delta v_i(k) \le \Delta v_{\max} \\ & v_{\min} \le \bar{I}\Delta v_{ik}(k) + 1_{N_c} \otimes v_i(k-1) \le v_{\max} \\ & \mathcal{Y}_{i\min} \le \Lambda_i \bar{x}(k|k) + \Psi_i \Delta u_i(k) \le \mathcal{Y}_{i\max} \end{array} \tag{19}$$

Hence, the existing active set method and interior point algorithm can be employed directly to solve the QP problem (17) and (19). Based on the MPC theory, the real-time optimal control input can be given by

$$v_d(k) = v(k-1) + \Delta v^*(k|k) \tag{20}$$

By repeating the above optimization process, the desired velocities can be further integrated to be the desired displacements for motion and formation systems.

ATSMC-based Dynamics Controller

As previously mentioned, to improve the robustness of the leader and further to enhance the adaptivity for the whole formation system, The ATSMC is presented to deal with the external uncertainty disturbance which will unavoidably impact upon the leader agent. The dynamic model (4) with an equivalent friction disturbance can be rewritten as

$$\bar{M}(q)\dot{v} = \bar{B}(q)\tau - F \tag{21}$$

where $F = [fv, f\omega]^T$ represents the wheel-ground friction disturbance. Defining a new state variate $z = [x_v, \theta]^T$, where x_v and θ are the displacement coordinate along the forward direction and the heading angle, respectively. Then, the system (21) can be transformed to a new dynamic system based on the robot displacement message, as follows

$$D(q)\ddot{z} + \bar{F} = u \tag{22}$$

where $D(q) = \mathrm{diag}(m, (J - md^2)/R)$ is the inertia matrix, $u = [u_1, u_2]^T$ is the new control input where $u_1 = (\tau_l + \tau_r)/r$ and $u_2 = (\tau_l - \tau_r)/r$, $\bar{F} = [f_v, f_\omega/R]^T$ is a new wheel-ground friction disturbance after a simple transformation. Furthermore, to establish trajectory tracking dynamic controller, and then the desired values of the system (22) can be defined as $z^d = [x_v^d, \theta^d]^T$, the differential of z^d can be expressed as $\dot{z}^d = v_l^d = [v_l^d, \omega_l^d]^T$. Using $e = [e_1, e_2]^T = z - z^d$ to represent the tracking errors, it is easy to obtained that $\dot{e} = \dot{z} - \dot{z}^d = v - v_l^d$ and $\ddot{e} = \ddot{z} - \ddot{z}^d = \dot{v} - \dot{v}_l^d$ afterward.

Lemma 3.2 Consider a first order system as $\dot{x} = u$. For achieving the finite convergence time, the closed-loop control will be globally asymptotically stable with the non-smooth controller as $u = -k\mathrm{sig}^\alpha(x)$, where $\mathrm{sig}^\alpha(x) = \mathrm{sgn}(x)|x|^\alpha$ with $0 < \alpha < 1$, $k > 0$, and the $\mathrm{sgn}(\cdot)$ represents a symbolic function.

By substituting the presented controller into the first order system, the closed-loop system can be achieved as $\dot{x} = -k\mathrm{sig}^\alpha(x)$. Then, the solution for the system can be formulated by

$$x(t) = \begin{cases} \mathrm{sgn}(x(0))[|x(0)|^{1-\alpha} - k(1-\alpha)t]^{\frac{1}{1-\alpha}}, & 0 < t \le \frac{|x(0)|^{1-\alpha}}{k(1-\alpha)} \\ 0, & t > \frac{|x(0)|^{1-\alpha}}{k(1-\alpha)} \end{cases} \tag{23}$$

With above preparation, a terminal sliding mode surface can be given by

$$s = \dot{e} + NE, \dot{E} = \mathrm{sig}^{\gamma}(e) \tag{24}$$

where $\mathrm{sig}^{\gamma}(e) = \mathrm{sgn}(e)|e|^{\gamma}$, $N = \mathrm{diag}(n_1, n_2)$ is the symmetric positive definite matrix; $s = [s_1, s_2]^T$ and $\gamma = \mathrm{diag}(\gamma_1, \gamma_2)$, where $0 < \gamma_1 < 1$ and $0 < \gamma_2 < 1$. If the index reaching law is employed, then the dynamic controller of the system (22) can be obtain as

$$u = -K_w s - K_v \mathrm{sgn}(s) + D(q)\ddot{z}_d - D(q)N\dot{E} + \bar{F} \tag{25}$$

where $K_w = \mathrm{diag}(k_{w1}, k_{w2})$ and $K_v = \mathrm{diag}(k_{v1}, k_{v2})$ are both positive definite matrix, with K_{w1},K_{w2},K_{v1} and K_{v2} are all positive design parameters.

Noticed that the friction disturbance $\bar{F}$ in controller (25) is unavailable in practice, which results in that the controller cannot be applied. To overcome this drawback, the adaptive law, as a soft-measurement method, need to be proposed to update the true values online. Then, defining $\hat{\bar{F}}$ as the estimated value of the $\bar{F}$, and the estimated error can be obtained as $\tilde{\bar{F}} = \hat{\bar{F}} - \bar{F}$ in the following. Regarding the slow time-varying behaviors of the friction feature, it holds that $\dot{\bar{F}} \approx 0$ and $\dot{\tilde{\bar{F}}} = \dot{\hat{\bar{F}}}$. Therefore, the presented ATSMC can be improved as

$$u = -K_w s - K_v \mathrm{sgn}(s) + D(q)\ddot{z}_d - D(q)N\dot{E} + \hat{\bar{F}} \tag{26}$$

where the adaptive law can be formulated by

$$\dot{\hat{\bar{F}}} = -\mu s \tag{27}$$

with the design parameter $\mu > 0$ determining the convergence time of the estimate value $\hat{\bar{F}}$. In general, increasing μ will accelerates the convergence rate of $\hat{\bar{F}}$.

Theorem 3.3 For the system (22), if the sliding mode manifold is defined as (24), then the dynamic controller can be given by (26) with adaptive law (27), such that all the signals in closed-loop system are bounded and the tracking errors will rapidly converge to zero within a finite time.

Proof. Considering a positive Lyapunov candidate as follows

$$V = \frac{1}{2} s^T D(q) s + \frac{1}{2\mu} \tilde{\bar{F}}^T \tilde{\bar{F}} \tag{28}$$

Differentiating V with respect to time yields

$$\begin{aligned}\dot{V} &= s^T D(q)(\ddot{e} + N\dot{E}) + \tfrac{1}{\mu}\tilde{\bar{F}}^T\dot{\bar{F}} \\ &= s^T(u - \bar{F} - D(q)\dot{v}_d + D(q)N\mathrm{sig}^y(e)) + \tfrac{1}{\mu}\dot{\bar{F}}\tilde{\bar{F}}^T\end{aligned} \tag{29}$$

Then, substituting controller (26) and adaptive law (27), it results in

$$\begin{aligned}\dot{V} &= s^T[-K_w s - K_v \mathrm{sgn}(s) + \hat{\bar{F}} - \bar{F}] + \tfrac{1}{\mu}\dot{\bar{F}}\tilde{\bar{F}}^T \\ &= s^T[-K_w s - K_v \mathrm{sgn}(s) + \tilde{\bar{F}}] + \tfrac{1}{\mu}\dot{\bar{F}}\tilde{\bar{F}}^T \\ &= -s^T K_w s - s^T K_v \mathrm{sgn}(s) + s^T\tilde{\bar{F}} + \tfrac{1}{\mu}(-\mu s)^T\tilde{\bar{F}} \\ &= -s^T K_w s - s^T K_v \mathrm{sgn}(s) \\ &\le 0\end{aligned} \tag{30}$$

By Lyapunov stability theorem and LaSalle invariance principle, it concludes that all the signals in the closed-loop system are bounded and the tracking errors will converge to zero as time goes by. Moreover, according to the finite time formula (23) of the Lemma 1, the finite times t_s can be governed by

$$t_s = \begin{bmatrix} t_{fv} \\ t_{f\omega} \end{bmatrix} = \left[\frac{|\dot{e}_1(0)|^{1-\gamma_1}}{n_1(1-\gamma_1)}, \frac{|\dot{e}_2(0)|^{1-\gamma_2}}{n_2(1-\gamma_2)} \right]^T \tag{31}$$

where t_{fv} and $t_{f\omega}$ are the terminal times for the respective subsystems. □

Simulation Results

To verify the effectiveness and feasibility of the proposed composite controller, the numerical simulations are developed in this section under Matlab environment. Assuming that a formation with one WMR as leader and two WMRs as followers, in which both leader and followers have the same mechanical structure parameters, as follows: $m = 6$ kg, $R = 0.25$ m, $r = 0.2$ m, $d = 0.1$ m, $J = 5$ kg $\cdot$ m^2. Here, the reference trajectory for leader given by the earth-fixed frame is supposed to be a circular path, with start point $(10, 0)$ and the radius is 10 m. The circular trajectory can be expressed as

$$\begin{cases} x_r &= 10 + 10\sin(0.2t) \\ y_r &= 10 - 10\cos(0.2t) \\ \theta_r &= 0.2t \end{cases} \tag{32}$$

The reference linear velocity and angle velocity of the leader are $v_l^r = \sqrt{\dot{x}_r^2 + \dot{y}_r^2} = 2$m/s and $\omega_l^r = 0.2$rad/s, respectively. The initial posture coordinate of the leader is $[x_l, y_l, \theta_l]^T = [11, -1, \pi/7]^T$, and the initial posture error is $[e_{xl}, e_{yl}, e_{\theta l}]^T = [1, -1, \pi/7]^T$. As for the formation configuration, the desired value of formation states are $[\rho_{l1}^d, \psi_{l1}^d, \beta_{l1}^d]^T = [1, \pi/2, 0]^T$

and $[\rho_{l2}^d, \psi_{l2}^d, \beta_{l2}^d]^T = [1, -\pi/2, 0]^T$ for follower 1 and 2, respectively; their initial states are $[\rho_{l1}, \psi_{l1}, \beta_{l1}]^T = [3, 7\pi/12, \pi/10]^T$ and $[\rho_{l2}, \psi_{l2}, \beta_{l2}]^T = [3, -7\pi/12, -\pi/10]^T$. Then the reference velocities of follower 1 and 2 are $v_1 = [v_1, \omega_1]^T = [1.8, 0.2]^T$ and $v_2 = [v_2, \omega_2]^T = [2.2, 0.2]^T$. Also, the parameters of MPC controllers are set as follows: the sampling time is $T = 0.1s$, the control horizon is $N_c = 10$, and the predictive horizon is $N_p = 30$. The weighting matrices are $Q_l = \mathrm{diag}(1, 1, 1)$ and $R_l = \mathrm{diag}(1, 1)$ for leader; $Q_1 = \mathrm{diag}(1, 1, 1)$, $R_1 = \mathrm{diag}(1, 1)$ for follower 1; $Q_2 = \mathrm{diag}(1, 1, 1)$, $R_2 = \mathrm{diag}(1, 1)$ for follower 2. Moreover, the dynamic controller parameters of the leader are given as follows: $\gamma_1 = \gamma_2 = 0.5$, $N = \mathrm{diag}(0.01, 0.01)$, $K_w = \mathrm{diag}(20, 5)$, $K_v = \mathrm{diag}(40, 20)$, and $\mu = \mathrm{diag}(300, 300)$. Meanwhile, for verifying the robustness of the presented controllers, a complicated external disturbance is introduced as

$$\bar{F} = \begin{bmatrix} 0.2 + 0.2\sin(2t) + 20\exp(-(t-12)^2/2h^2) \\ 0.2 + 0.2\sin(2t) + 20\exp(-(t-22)^2/2h^2) \end{bmatrix} \tag{33}$$

This disturbance includes constant function, sinusoidal function and Gauss function, representing invariable, gradual and mutational changes from the uncertain environment, respectively. In this case, the Gauss function is supposed to occur in 12 and 22 s on left and right wheels with the parameter $h = 0.5$ m.

The time responses of trajectory tracking for the formation with or without compensation are shown as Figures 3–4, where the roundness means the start point and the squares represents the end point of the leader and followers. More specifically, form Figure 3, it suggests that at the effect of MPC-based controller, both follower 1 and follower 2, including the leader, can maintain the desired formation with a favorable dynamic performance even though in a circumstance existing disturbance. Nevertheless, as illustrated in Figure 4, the leader without adaptive compensation exhibits an large deviating from the reference trajectory exactly, together with the two followers undergoing a similar process of departure.

Furthermore, to exhibit the tracking performance for leader, the time responses of the tracking errors with or without adaptive compensation are shown in Figures 5–6, respectively. The results shown in Figure 5 indicate that during a period about 5 s, all tracking errors converge to the required compact sets. Also, the partial enlarged drawing reveals that all errors are restricted within 0.05 and the errors will converge to be a compact sets again after a period of regulation. As a result, the closed-loop trajectory tracking control system for leader is verified to be stable with a satisfactory performance. However, as plotted in Figure 6, if the compensation is not adopted, the errors caused by f_v ($t = 12$s) and f_w ($t = 22$s) are such violent causing the leader nearly cannot track the reference trajectory.

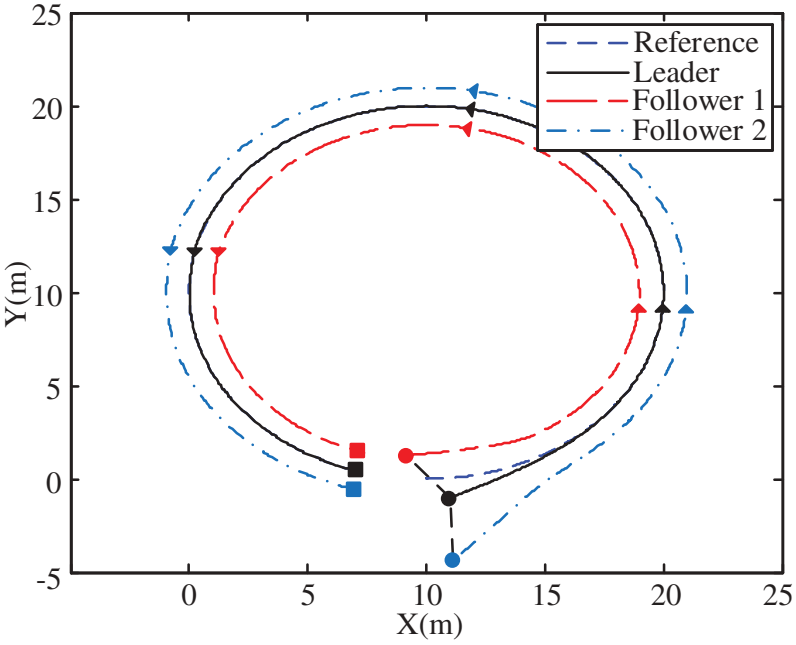

Figure 3. Trajectory tracking with compensation.

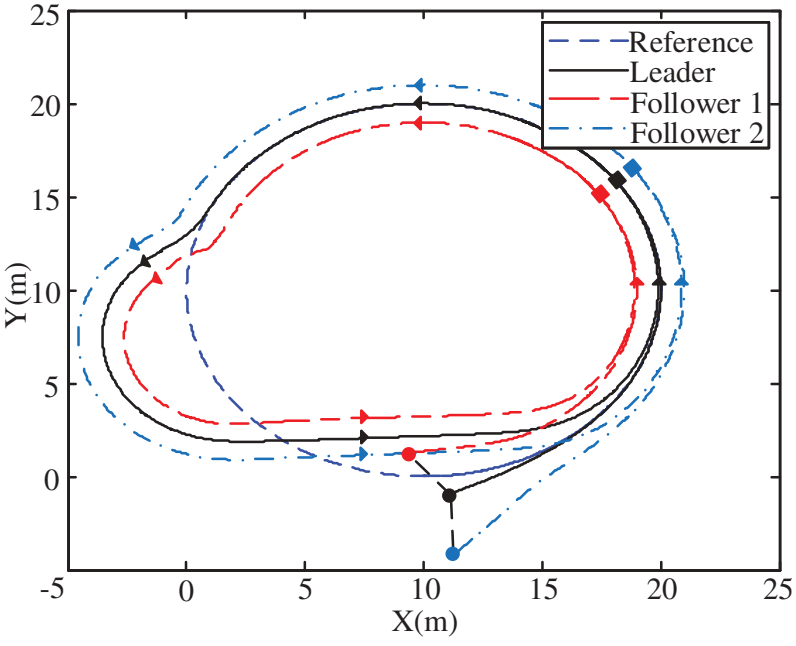

Figure 4. Trajectory tracking without compensation.

What is more, as shown in Figure 7, although there exists external disturbance acting on the leader, the formation errors, i.e., e_ρ, e_ψ, and e_β, are very small, especially for the distance error e_ρ. As for bearing angle error

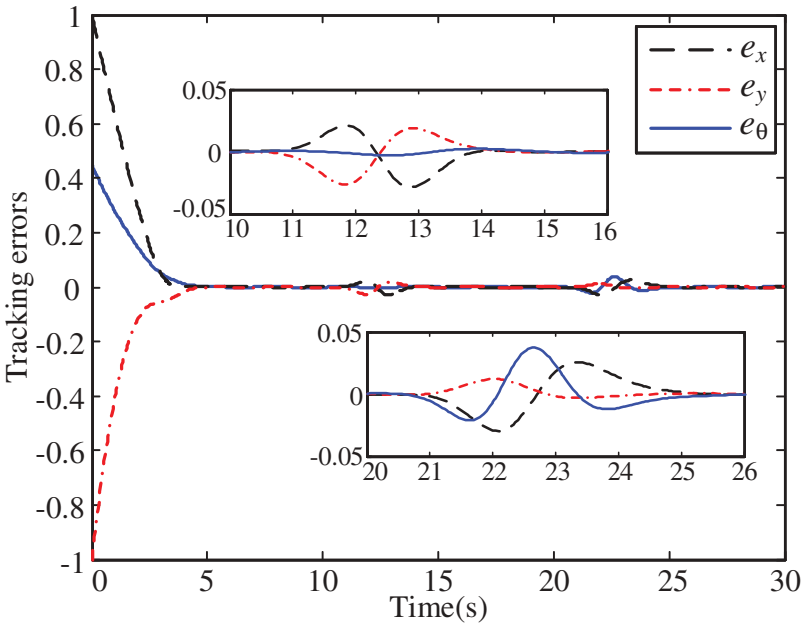

Figure 5. Leader tracking errors with compensation.

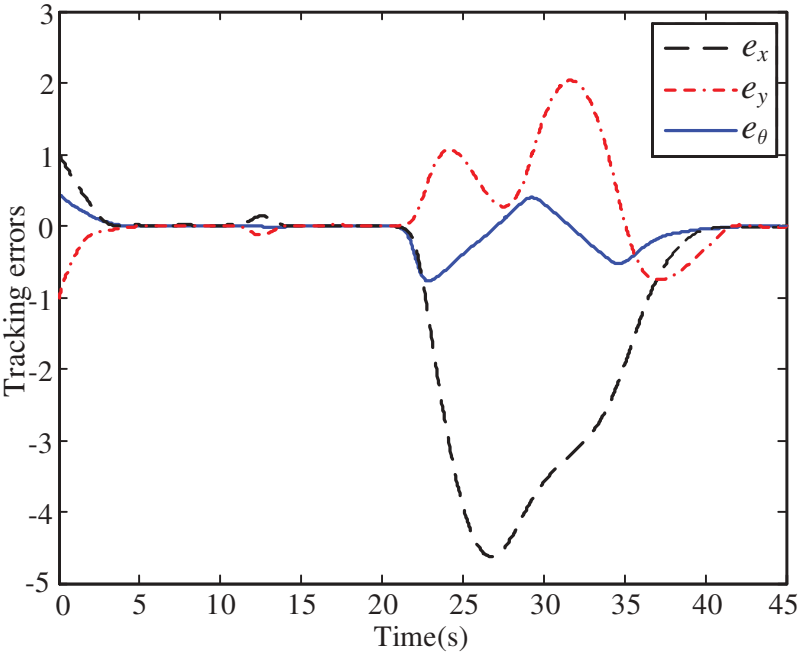

Figure 6. Leader tracking errors without compensation.

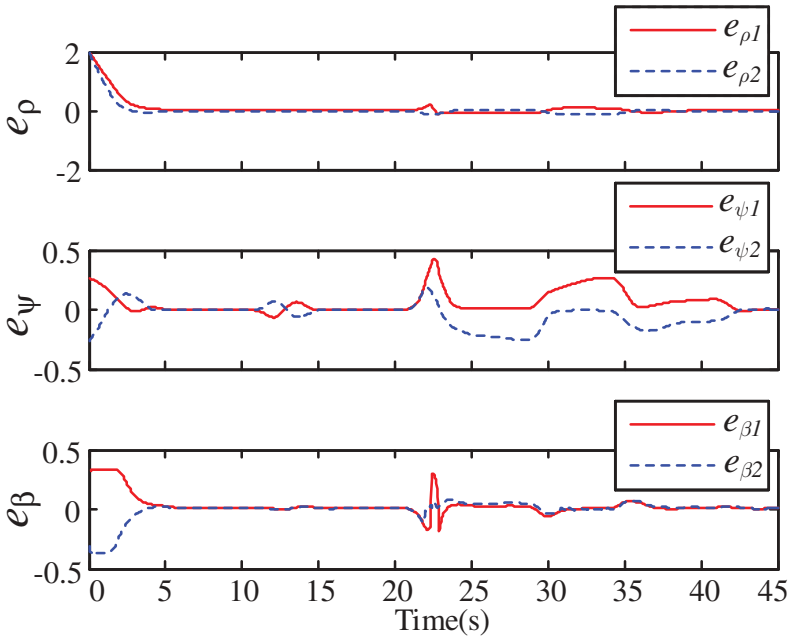

Figure 8. Formation errors without compensation.

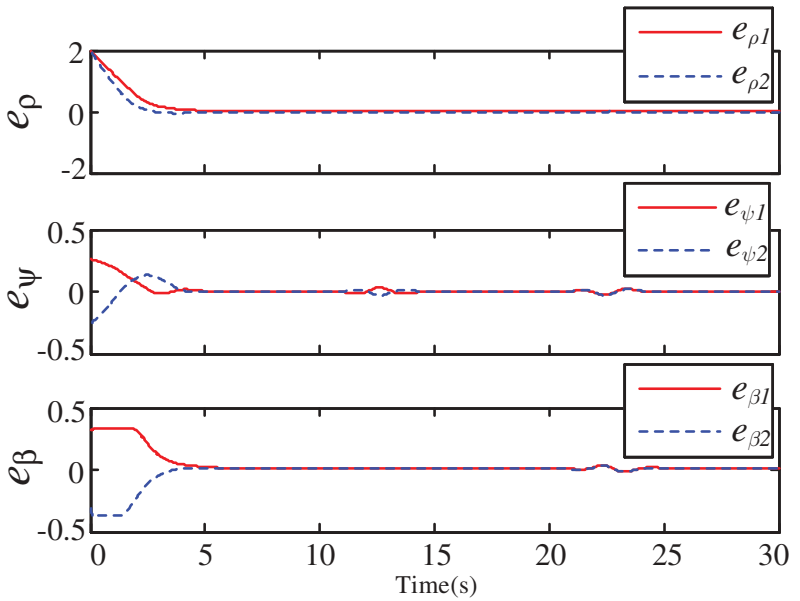

Figure 7. Formation errors with compensation.

e_ψ and heading angle error e_β, a tiny chattering takes place as the appearance of Gauss function at 12 and 22 s, and the chattering will vanish quickly after a limited time. For comparison, as plotted in Figure 8, the formation errors without compensation are more difference: e_ρ is relatively small in the

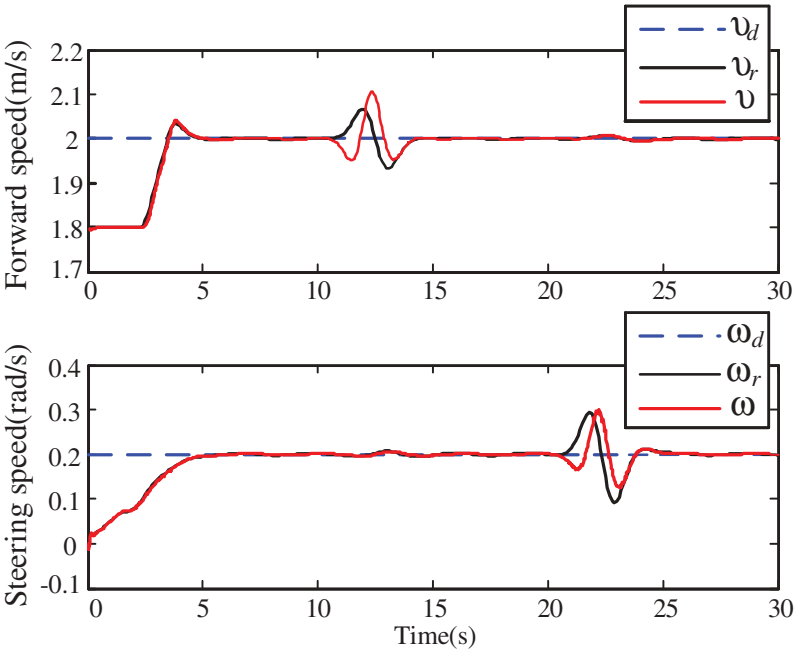

Figure 9. Response of leader's velocity tracking.

presence of f_v (t = 12 s) and f_ω (t = 22 s), but for e_ψ and e_β, dramatic chattering will occur and last a longer time, especially f_ω taking place.

In addition, the time response of velocity tracking for leader and followers are shown, respectively, in Figures 9–10. The results in Figure 9 tell that, the v_l^d and ω_l^d controlled by MPC-based motion controller will converge to the reference value v_l^r and ω_l^r within about 5 s. Preferably, the v_l and ω_l controlled by ATSMC-based dynamics controller converges to the v_l^d and ω_l^d with a faster time period. Moreover, despite of the Gauss disturbance acting at 12 and 22 s, all signals are convergence to the desired values within 4 s. As shown in Figure 10, both forward speeds and steering speeds of the two followers are stabilized to desired value without any chattering in the first 5 s, but when the f_v and f_ω occur, both of the velocities exhibit somewhat fluctuation and will vanish quickly.

As illustrated in Figure 11, the time responses of disturbance estimation, in addition to the estimation errors, are provided to illustrate the effectiveness of the proposed ATSMC controller. It demonstrates that both f_v and f_ω can approach their true value f_{vd} and $f_{\omega d}$, respectively, with in a short time. Specifically, when the Gauss disturbance arises at 12s and 22s, the errors have a fluctuation within 2N for f_v and 0.6N for f_ω, and the vibrational amplitudes are suppressed to an acceptable bound within 4 s.

In addition, the control inputs are shown in Figure 12, whose results reveal that the system controls adaptively change according to the external

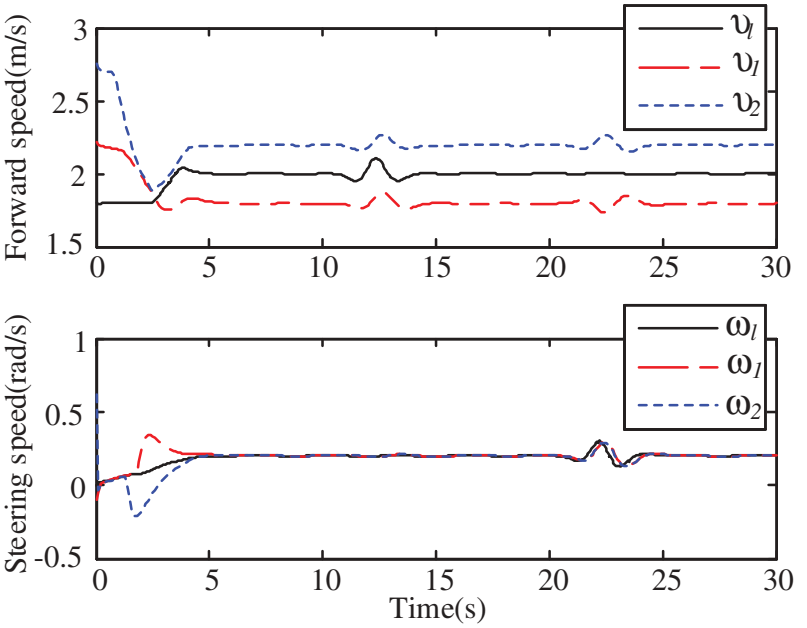

Figure 10. Response of followers' velocity tracking.

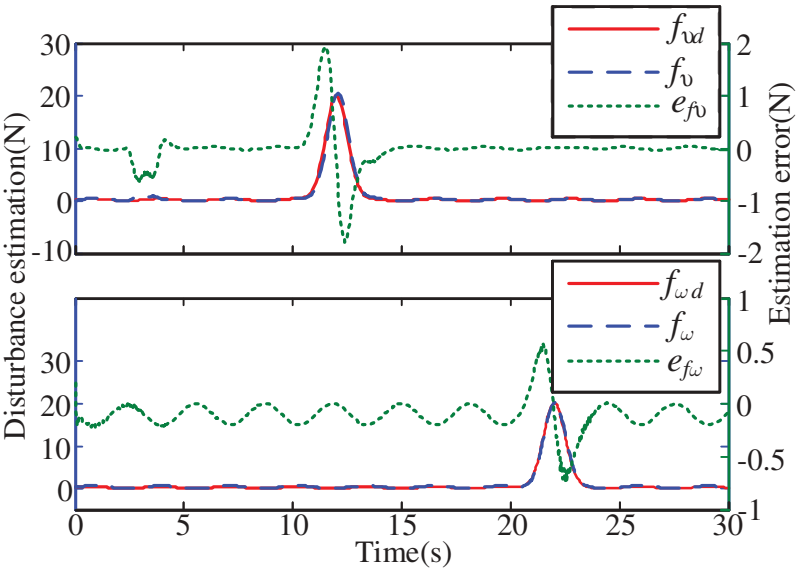

Figure 11. Disturbance estimation and its errors.

disturbance. Meanwhile, at the impact at 12 and 22 s, the control inputs have an oscillation with the amplitude 6N, and afterward within 4 s, the changing tendency agrees well with the uncertain dynamics. The stability of the control signals guarantees the feasibility of the proposed ATSMC-based controller.

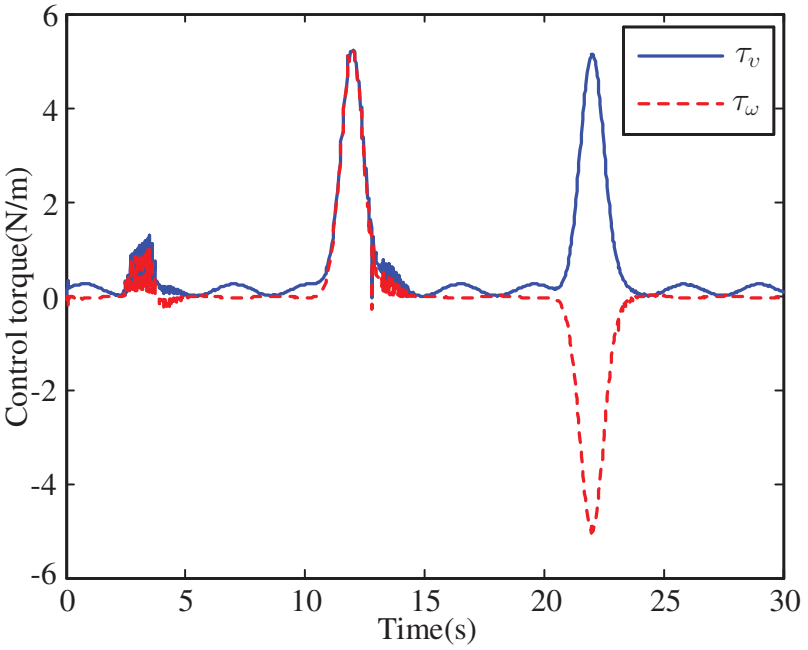

Figure 12. Time responses of control torque.

Conclusion

In this paper, an effective composite control strategy based on the MPC and ATSMC methods is proposed to realize the formation control of the WMRs in the presence of external disturbance. Compared with the other existing control approaches, thanks to the ATSMC technique, the presented control method can estimate and compensate the disturbance for the leader agent quickly and robustly, thus guaranteeing the motion stability and accuracy of the entire-formation system due to the leader's significant role. Besides, another prominent advantages arise from the successfully utilizing the MPC control method, by which various constraints can be assured not only for the formation configuration but also for the agents' dynamic behaviors. Further work will develop the experimental studies for the proposed composite control strategy.

Funding

This work was supported in part by the National Natural Science Foundation of China under Grants (Nos. 61873047 and 61573078), in part by the Natural Science Foundation of Liaoning Province of China under Grant 20170540171, in part by the Fundamental Research Funds for the Central Universities under Grant DUT19ZD205, and in part by the State Key Laboratory of Robotics and System (HIT) under Grant SKLRS-2019-KF-17.

References

Cui, R. X., S. S. Ge, B. V. E. How, and Y. S. Choo. 2010. Leader–Follower formation control of underactuated autonomous underwater vehicles. *Ocean Engineering* 37:1491–502. doi:10.1016/j.oceaneng.2010.07.006.

Hong, Y. G., J. P. Hu, and L. X. Gao. 2006. Tracking control for multi-agent consensus with an active leader and variable topology. *Automatica* 42:1177–82. doi:10.1016/j.automatica.2006.02.013.

Hu, Q. L., Y. Meng, C. L. Wang, and Y. M. Zhang. 2018. Adaptive backstepping control for air-breathing hypersonic vehicles with input nonlinearities. *Aerospace Science and Technology* 73:289–99. doi:10.1016/j.ast.2017.12.001.

Hu, Q. L., Y. Y. Liu, and Y. M. Zhang. 2019. Control of non-cooperative spacecraft in final phase proximity operations under input constraints. *Control Engineering Practice* 87:83–96. doi:10.1016/j.conengprac.2019.04.001.

Ke, F., Z. J. Li, H. Z. Xiao, and X. B. Zhang. 2017. Visual servoing of constrained mobile robots based on model predictive control. *IEEE Transactions on Systems, Man, and Cybernetics: Systems* 47:1428–38. doi:10.1109/TSMC.2016.2616486.

Li, H. Y., P. Shi, and D. Y. Yao. 2017. Adaptive sliding-mode control of Markov jump nonlinear systems with actuator faults. *IEEE Transactions on Automatic Control* 62:1933–39. doi:10.1109/TAC.2016.2588885.

Li, Z. J., J. Deng, R. Q. Lu, Y. Xu, J. J. Bai, and C. Y. Su. 2016. Trajectory-tracking control of mobile robot systems incorporating neural-dynamic optimized model predictive approach. *IEEE Transactions on Systems, Man, and Cybernetics: Systems* 46:740–49. doi:10.1109/TSMC.2015.2465352.

Pan, H. H., W. C. Sun, H. J. Gao, and J. Y. Yu. 2015. Finite-time stabilization for vehicle active suspension systems with hard constraints. *IEEE Transactions on Intelligent Transportation Systems* 16:2663–72. doi:10.1109/TITS.2015.2414657.

Peng, Z. X., G. G. Wen, A. Rahmani, and Y. G. Yu. 2013. Leader-follower formation control of nonholonomic mobile robots based on a bioinspired neurodynamic based approach. *Robotics & Autonomous Systems* 61:988–96. doi:10.1016/j.robot.2013.05.004.

Peng, Z. X., S. C. Yang, G. G. Wen, A. Rahmani, and Y. G. Yu. 2016. Adaptive distributed formation control for multiple nonholonomic wheeled mobile robots. *Neurocomputing* 173:1485–94. doi:10.1016/j.neucom.2015.09.022.

Qin, J. H., and C. B. Yu. 2013. Cluster consensus control of generic linear multi-agent systems under directed topology with acyclic partition. *Automatica* 49:2898–905. doi:10.1016/j.automatica.2013.06.017.

Qin, J. H., H. J. Gao, and W. X. Zheng. 2012. Consensus strategy for a class of multi-agents with discrete second-order dynamics. *International Journal of Robust and Nonlinear Control* 22:437–52. doi:10.1002/rnc.v22.4.

Ren, W., and N. Sorensen. 2008. Distributed coordination architecture for multi-robot formation control. *Robotics and Autonomous Systems* 56:324–33. doi:10.1016/j.robot.2007.08.005.

Sun, X. M., and W. Wang. 2012. Integral input-to-state stability for hybrid delayed systems with unstable continuous dynamics. *Automatica* 48:2359–64. doi:10.1016/j.automatica.2012.06.056.

Sun, Y. W., M. S. Chen, J. J. Jia, Y. S. Lee, and D. M. Guo. 2019. Jerk-limited federate scheduling and optimization for five-axis machining using new piecewise linear programming approach. *Science china technological sciences*, 1–15. doi:10.1007/s11431-018-9404-9.

Wang, D., N. Zhang, J. L. Wang, and W. Wang. 2017. A PD–Like protocol with a time delay to average consensus control for multi-agent systems under an arbitrarily fast switching topology. *IEEE Transactions on Cybernetics* 47:898–907. doi:10.1109/TCYB.2016.2532898.

Wang, R., X. W. Dong, Q. D. Li, and Z. Ren. 2016. Distributed adaptive time-varying formation for multi-agent systems with general high-order linear time-invariant dynamics. *Journal of the Franklin Institute* 353:2290–304. doi:10.1016/j.jfranklin.2016.03.016.

Wang, W., D. Wang, and Z. H. Peng. 2017. Fault-tolerant containment control of uncertain nonlinear systems in strict-feedback form. *International Journal of Robust and Nonlinear Control* 27:497–511. doi:10.1002/rnc.v27.3.

Wang, W., D. Wang, and Z. H. Peng. 2017. Fault-tolerant containment control of uncertain nonlinear systems in strict-feedback form. *International Journal of Robust and Nonlinear Control* 27:497–511. doi:10.1002/rnc.v27.3.

Wang, X. Y., S. H. Li, and P. Shi. 2014. Distributed finite-time containment control for double-integrator multiagent systems. *IEEE Transactions on Cybernetics* 44:1518–28. doi:10.1109/TCYB.2013.2288980.

Xiao, B., S. Yin, and O. Kaynak. 2016. Tracking control of robotic manipulators with uncertain kinematics and dynamics. *IEEE Transactions on Industrial Electronics* 63:6439–49. doi:10.1109/TIE.2016.2569068.

Xiao, H. Z., Z. Li, and C. P. Chen. 2016. Formation control of leader–follower mobile robots systems using model predictive control based on neural-dynamic optimization. *IEEE Transactions on Industrial Electronics* 63:5752–62. doi:10.1109/TIE.2016.2542788.

Xu, L., Q. L. Hu, and Y. M. Zhang. 2017. L_2 performance control of robot manipulators with kinematics, dynamics and actuator uncertainties. *International Journal of Robust and Nonlinear Control* 27:875–93. doi:10.1002/rnc.3604.

Yang, C. G., C. Chen, N. Wang, Z. J. Ju, J. Fu, and M. Wang. 2019. Biologically-inspired motion modeling and neural control for robot learning from demonstrations. *IEEE Transactions on Cognitive and Developmental Systems* 11:281–291. doi:10.1109/TCDS.2018.2866477.

Yoo, S. J. 2017. A low-complexity design for distributed containment control of networked pure-feedback systems and its application to fault-tolerant control. *International Journal of Robust and Nonlinear Control* 27:363–79. doi:10.1002/rnc.v27.3.

Yu, W. W., G. R. Chen, and M. Cao. 2010. Distributed leader–Follower flocking control for multi-agent dynamical systems with time-varying velocities. *Systems & Control Letters* 59:543–52. doi:10.1016/j.sysconle.2010.06.014.

Yue, M. 2014. Disturbance observer-based trajectory tracking control for nonholonomic wheeled mobile robot subject to saturated velocity constraint. *Applied Artificial Intelligence* 28:751–765. doi:10.1080/08839514.2014.952918.

Yue, M. 2015. 1998. Adaptive fuzzy logic-based sliding mode control for a nonholonomic mobile robot in the presence of dynamic uncertainties. *Proceedings of The Institution of Mechanical Engineers* Part C. *Journal of Mechanical Engineering Science,* 229:1979–1988. doi:10.1177/0954406214551625.

Zhang, L. X., S. L. Zhuang, and R. D. Braatz. 2016. Switched model predictive control of switched linear systems: feasibility, stability and robustness. *Automatica* 67:8–21. doi:10.1016/j.automatica.2016.01.010.

Zhao, X. D., H. J. Yang, and G. D. Zong. 2016. Adaptive neural hierarchical sliding mode control of nonstrict-feedback nonlinear systems and an application to electronic circuits. *IEEE Transactions on Systems, Man, and Cybernetics: Systems* 47:1394–404. doi:10.1109/TSMC.2016.2613885.